Cement and Concrete Composites 148 (2024) 105477

Contents lists available at ScienceDirect

Cement and Concrete Composites

journal homepage: www.elsevier.com/locate/cemconcomp

Understanding the $CaCO_3$ phase transition of carbonated wollastonite composites caused by sodium tripolyphosphate: From amorphous to crystalline

Lulu Cheng [a], Yuxuan Chen [a,**], Tao Liu [b], H.J.H. Brouwers [b], Qingliang Yu [a,b,*]

[a] School of Civil Engineering, Wuhan University, Wuhan, 430072, PR China
[b] Department of the Built Environment, Eindhoven University of Technology, P.O. Box 513, 5600 MB, Eindhoven, the Netherlands

ARTICLE INFO

Keywords:
Calcium carbonate
Wollastonite
Sodium tripolyphosphate
Carbonation
Phase transition

ABSTRACT

Developing new cementitious materials through mineral carbonation attracts increasing attention for reducing carbon emissions. However, the role of $CaCO_3$ phase transition in the strength development of carbonated composites is not clear. In this study, new carbonated wollastonite composites are prepared and sodium tripolyphosphate (STPP) is used as a phase-controlling additive for the phase transition evolution of $CaCO_3$ polymorphs during the carbonation process. Moreover, mechanical performance, microstructure, and carbonation mechanism are investigated. Results show that STPP is effective in enhancing mechanical performance by controlling $CaCO_3$ phase transition. Specifically, STPP prolongs the phase transition of amorphous calcium carbonate (ACC) until 72 h later (the control binder at 1 h), allowing more opportunities for structural rearrangement. Besides, the introduction of STPP results in the formation of more stable ACC, vaterite, and aragonite, causing a compact microstructure and a lower carbonation degree. More importantly, STPP concentration within 0.3 M strongly improves the cementitious performance of all carbonated products (2.65–4.14 MPa/%), contributing to compressive strength growth (11.10–83.71%). The 0.1 M STPP-containing binder exhibits the highest compressive strength of 75.59 MPa. Our results contribute to unique pathways toward understanding the carbonation mechanism and a more sustainable cement industry.

1. Introduction

Accompanied with high natural resource consumption and high CO_2 emissions of ordinary Portland cement (OPC), the exploration and development of new cementitious material to reduce carbon footprint are imperative [1–4]. Previous studies have shown that amorphous calcium carbonate (ACC) is a key precursor phase in the biomineralization process of calcareous materials, and cementitious property is obtained via the crystallization transformation of ACC [5,6]. Inspired by these findings, calcium carbonate-based composite is expected to be a novel future cementitious material by controlling the crystallization transformation of ACC [7,8]. This binder can be prepared through CO_2-activated calcium-rich material in the presence of moisture [9–13]. Among all calcium-rich materials, wollastonite is a natural calcium silicate mineral, avoiding carbon emissions from calcination. Meanwhile, wollastonite is known as a non-hydraulic mineral and has higher carbonation reactivity [14–16], indicating that only the carbonation reaction occurs and there is no competition with the hydration reaction. Considering these factors, wollastonite is introduced as a calcium source for CO_2 fixation. This hardened matrix will be referred to as 'carbonated wollastonite composites' or 'carbonated composites' for the rest of this article.

The carbonated products of wollastonite are $CaCO_3$ and silica gel, which act as the cementitious phases and provide strength to the hardened matrix [17,18]. In general, $CaCO_3$ occurs naturally in seven different forms: amorphous $CaCO_3$ (ACC), three anhydrous polymorphs: calcite, aragonite, and vaterite, in the order of decreasing thermodynamic stability, as well as three hydrated crystals-monohydrocalcite ($CaCO_3{\cdot}H_2O$), ikaite ($CaCO_3{\cdot}6H_2O$) and hemihydrate ($CaCO_3{\cdot}1/2H_2O$) [19]. Due to the short-range disordered characteristic, ACC is easily molded into many different shapes by crystallization transformation [20]. ACC includes stable and transient forms. Transient ACC rapidly

* Corresponding author. School of Civil Engineering, Wuhan University, Wuhan, 430072, PR China.
** Corresponding author.
E-mail addresses: Yuxuan.chen@whu.edu.cn (Y. Chen), q.yu@bwk.tue.nl (Q. Yu).

https://doi.org/10.1016/j.cemconcomp.2024.105477
Received 6 October 2023; Received in revised form 26 January 2024; Accepted 13 February 2024
Available online 15 February 2024

transforms via dissolution-recrystallization mechanism while crystallization of stable ACC occurs via solid-state mechanism or particle attachment mechanism [21,22]. It is now known that many invertebrate organisms initially form ACC phase, which subsequently crystallizes to form skeletal parts [23]. The final crystalline phases are typically the mineral forms of $CaCO_3$: calcite or aragonite. In addition to these, the best characterized phase change system is the seashells and sea urchin embryo [24–27]. Calcite and ACC coexist in the seashells, and ACC precursors transform into calcite crystal over time [26,28]. Formed multiple $CaCO_3$ crystal microlayers are assembled to form their supporting structures. Such biomineralization has inspired the design of $CaCO_3$-based composites that may only be prepared using the crystallization transformation of ACC precursor. Besides, the intrinsic properties of $CaCO_3$ crystals are significantly different. As an example, the stiffness of vaterite, aragonite, and calcite are 39.13 GPa, 67 GPa and 72.83 GPa, respectively [29]. Therefore, the change in phase transition of ACC and the relative proportions of different $CaCO_3$ polymorphs often leads to significant variability in the mechanical performance of carbonated composites [30,31]. However, until now, most studies have focused on the effect of silica gel on strength development [10,32,33], and few studies have reported the contribution of ACC phase transition and polymorphs evolution to mechanical strength, as well as the preparation of new cementitious material by using $CaCO_3$ phase transition mechanism [34,35].

By controlling phase transition of $CaCO_3$, organic additives not only determine morphology, spatial arrangement, and crystal orientation of biomaterials, but also the mechanical properties of biomaterials [36–39]. In the biomineralization process, phosphate ions have proved to play a key role in the stabilization and transformation of ACC in living organisms, and a higher phosphate concentration shows a greater controlling crystallization advantage [40,41]. Thus, a polyphosphate chelating agent, sodium tripolyphosphate (STPP, chemical formula $Na_5P_3O_{10}$), is proposed [42]. As a hydrophilic polymer material, STPP can dissolve in water to form a solution, and then be adsorbed or self-assembled into aggregates through molecular design and optimization [43]. Specifically, STPP can stabilize ACC under heating and the higher concentration stabilizes it to a greater extent [44,45]. A small concentration inhibits the dissolution of vaterite and crystallization of calcite, which contributes to the stability of vaterite and sufficiently retards the crystallization of vaterite to allow the formation of cementitious behavior [43,46]. Our previous study [6] also suggested that $CaCO_3$ crystallizes in the presence of STPP via a multistep process, which leads us to speculate that it should be possible to control the transformation process of ACC and the morphology, structure, crystal orientation of $CaCO_3$ by varying STPP amount so as to control cementitious behavior of binder. Nevertheless, the research on STPP-induced formation of carbonated wollastonite composites is rare, let alone explaining the carbonation mechanism of how phase transition of ACC and the formation of different $CaCO_3$ controlled by STPP produces cementitious performance and contributes to the formation of mechanical properties.

Inspired by biomineralization, STPP is selected as an ACC phase change and $CaCO_3$ polymorph controlling additive, and a high-performance carbonated wollastonite composite is prepared. The formation and evolution of $CaCO_3$ polymorph are explored by infrared spectroscopy (FT-IR), X-ray diffraction (XRD) and thermogravimetric analysis (TGA) analyses. The macroscopic mechanical properties and microstructure of this binder are systematically characterized by compressive strength, mercury intrusion porosimetry (MIP), and scanning electron microscope (SEM) tests. This study devotes to the preparation of a novel carbon-negative cement by controlling $CaCO_3$ phase transition, and the proposed carbonation mechanism is helpful to the design and development of long-term performance of $CaCO_3$-based binder.

2. Materials and methods

2.1. Materials

2.1.1. Mineral precursor

The main raw material used in this work was wollastonite, which was supplied from South Wollastonite Co.LTD (China) and was a fine powder with a BET surface area of 6.29 m^2/g determined by TriStar II 3020 High Throughput Surface Area and Porosity Analyzer. Table 1 illustrates the chemical composition of wollastonite as detected by X-ray fluorescence (XRF), combined with the X-ray powder diffraction (XRD) (Fig. 1) results. The ground powder consists mainly of wollastonite (wollastonite 1A, space group: $P\bar{1}$, $a = 7.934$ Å, $b = 7.334$ Å, $c = 7.075$ Å, $\alpha = 89.95°$, $\beta = 95.26°$, $\gamma = 103.45°$) and small amounts of wollastonite 2 M (parawollastonite, space group: $P21$, $a = 15.429$ Å, $b = 7.3251$ Å, $c = 7.0692$ Å, $\alpha = 90.00°$, $\beta = 95.38°$, $\gamma = 90.00°$). From TG results (Fig. 2a), it can be observed that about 9.49% of wollastonite is unavoidably carbonated, which provides evidence for LOI results. Fig. 2b shows the particle size distribution (PSD) as determined by Mastersizer 2000, applying the wet method with water as a dispersant (refractory index of 1.52). The wollastonite presents a small particle distribution ranging from 0.3 to 200 μm. Specifically, the PSD parameters, including D_{10}, D_{50}, D_{90}, are 0.893 μm, 4.525 μm, and 28.286 μm, respectively.

2.1.2. Performance-controlling additive

STPP, an amorphous water-soluble linear polyphosphate [42], was used as the chelating agent for ACC phase change and $CaCO_3$ polymorph controlling additive. STPP solution was prepared by dissolving analytical-grade sodium tripolyphosphate (obtained from Sinopharm Chemical, China) in ultrapure water.

2.2. Sample preparation

2.2.1. Wollastonite dissolution

To investigate the effect of STPP on the carbonation kinetic of carbonated wollastonite composites, three STPP solutions with various concentrations (0.1 M, 0.2 M, and 0.3 M) were used. The fresh pastes were prepared at a constant liquid-to-solid mass ratio (STPP/wollastonite) of 0.39. Then, the raw materials, including wollastonite powder and STPP solution, were stirred for at least 5 min. A control sample was prepared by mixing ground wollastonite with water at the same liquid-to-solid ratio.

2.2.2. Wollastonite carbonation

For in-situ monitoring $CaCO_3$ polymorph evolution over carbonation time and further revealing the carbonation process of carbonated wollastonite composites, the fresh pastes with 1–3 mm thickness were spread on plastic plates to eliminate the influence of specimen thickness on CO_2 diffusion. Carbonation reactions were performed at the condition: 30 °C, 80% RH, and 20% CO_2 through a commercial carbonation chamber. The carbonated samples were collected at different time intervals of 0, 30 min, 1 h, 9 h, 24 h, 72 h, and 120 h. Afterwards, some sample surfaces were immediately sprayed with a 1% phenolphthalein pH indicator to recognize color change, and others were rinsed twice with absolute ethyl alcohol to terminate reaction. These solids were dried in a vacuum drying oven at 40 °C for 24 h and then stored in a vacuum desiccator for subsequent characterizations.

The remaining pastes were cast into 20 × 20 × 20 mm^3 cube molds for mechanical strength and pore structure testing. These samples were vibrated with a shaking table for 1 min to remove the bubbles in the slurry and immediately moved to carbonation chamber, the same one as described for thin paste. They were de-molded after 24 h carbonation curing, and then cured at the same carbonation conditions until 3 days, 14 days and 28 days.

Table 1
Chemical composition of wollastonite (wt.%).

Oxides	MgO	Al_2O_3	SiO_2	P_2O_5	SO_3	K_2O	CaO	Fe_2O_3	LOI
Wollastonite	0.62	0.14	43.94	0.03	0.03	0.03	42.72	0.18	12.23

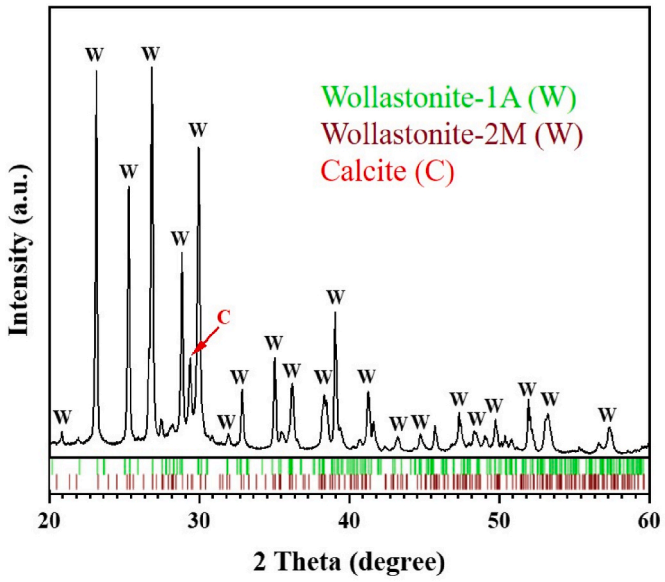

Fig. 1. XRD pattern of wollastonite.

2.3. Test methods

2.3.1. Carbonated products identification and quantification

To monitor $CaCO_3$ polymorph evolution, the Fourier-Transformed Infrared spectra (FT-IR) and X-ray Diffraction (XRD) patterns of the carbonated product were collected. FT-IR spectra were recorded using a Thermo Scientific Nicolet IS 5 FT-IR spectrometer by the method of tableting with potassium bromide. All spectra were scanned 32 times from 4000 to 400 cm^{-1} with 4 cm^{-1} resolutions. XRD patterns of the ground paste sample were determined via a MiniFlex600 X-ray powder diffractometer (made by Rigaku) using Cu-Kα radiation. The diffraction patterns were obtained between 2θ range from 5° to 65° in continuous mode with a step scan speed of 0.02°/s. The PDF card numbers used were as follows: PDF #05-0586 for calcite, PDF #75-2230 for aragonite, PDF #74-1867 for vaterite, PDF #43-1460 for wollastonite.

To further provide a semi-quantification for carbonated products during different carbonation duration, TG analysis was conducted using a synchronous thermal analyzer (TA instrument, SDT 650) with N_2 as the protective gas by heating up to 1000 °C from 30 °C at the rate of 10 °C/min. Moreover, the amount of silica gel formed in the carbonation process was determined by the hydrochloric acid (HCl) dry-fixing method and TG results. The carbonated products of wollastonite were $CaCO_3$, silica gel, and unreacted $CaSiO_3$, in which the reactions of carbonated products and HCl include: i) $CaCO_3 + 2HCl \rightarrow CaCl_2 + CO_2 + H_2O$; ii) $CaSiO_3 + 2HCl \rightarrow CaCl_2 + SiO_2 \bullet H_2O$, and silica gel do not react with HCl. Specific experimental methods are as follows: (1) The carbonated products were ground into a fine powder with a particle size of less than 75 μm. (2) Solid power (0.5 g) and HCl solution (10 wt %, 40 g) were mixed and stirred in the beaker for 30 min (3) After the reaction was achieved, precipitates were collected through fast vacuum filtering of 0.2 μm millipore membrane and rinsed twice with deionized water to remove impurities. (4) The obtained solids were dried in a vacuum drying oven at 60 °C to constant weight, which was the total mass of silica gel formed by carbonated wollastonite and the acid dissolution of unreacted wollastonite. Based on TG and the experimental results, the carbonation reaction equation of wollastonite is obtained and verified, as shown in Eq. (2). The amounts of different carbonated products are calculated and detailed results are shown in Section 3.3.

$$CaSiO_3 + CO_2 + H_2O \rightarrow CaCO_3\downarrow + SiO_2 \bullet H_2O \quad (2)$$

2.3.2. Microstructure characterization

Scanning Electron Microscopy (SEM) and elemental dispersive X-ray spectroscopy (EDS) analyses were carried out using a Zeiss Sigma field emission SEM instrument to investigate microstructure of the binder. It was operated in high-vacuum mode and worked at an accelerating voltage of 5 kV and a working distance of 10 mm. The particle surface was coated with gold-palladium to facilitate charge dissipation. Also, to study the effect of STPP on the morphology of wollastonite minerals, wollastonite was immersed in STPP solutions for 60 days and then was dried for 24 h in a vacuum oven at 40 °C for SEM analysis.

AutoPore IV instrument (Micrometritics) was used to analyze the pore structure of the hardened matrix. Before characterization, the 28-day carbonation cured binder was processed into granular particles with a size range of 1–3 mm, and then dried at 105 °C in a vacuum

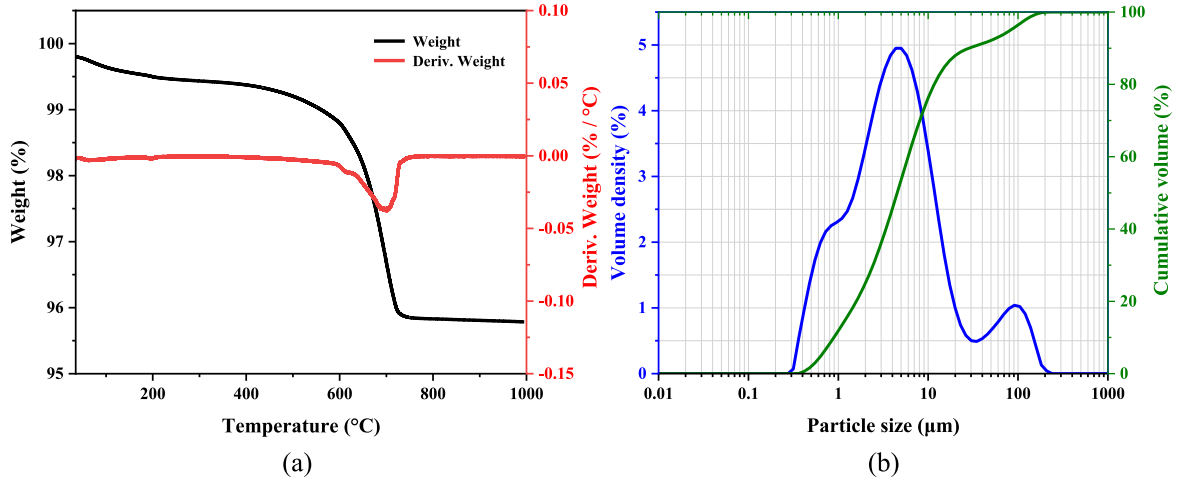

Fig. 2. (a) TG curves; (b) Particle size distribution.

environment to eliminate the influence of internal moisture.

2.3.3. Mechanical properties

Workability of carbonated binder was performed by the mini spread-flow test. Fresh paste was placed into a normal conical ring and followed by a 25 jolting. The diameter of carbonated binder was measured 4 times after jolting and the average value was denoted as the slump flow.

The compressive strength of the hardened binder was determined by using a servo-hydraulic pressure testing machine capable of a maximum force value of 100 kN based on the principle of unrestricted compression test. The constant loading speed was 0.8 mm/min. Three replicate samples of each mixture were used to calculate the average value.

3. Results

3.1. Time-dependent carbonation degree and mechanical performance

Fig. 3 shows the color variation of carbonated wollastonite composites after different carbonation durations, recognized by the phenolphthalein pH-indicator [47]. As a salt substance, STPP contains many negatively charged phosphate ions. These ions interact with water molecules, causing H^+ of water molecules to gradually consume and the pH of water to become higher. As a result, STPP is alkaline and is the only alkaline source in this system. Thus, all STPP-containing samples exhibit pink after spraying the phenolphthalein indicator and the intensity of pink color has a strong relationship with the STPP amount. Specifically, the pink color of carbonated materials at the same carbonation time tends to be darker along with the increased STPP. Moreover, the color of all binders undergoes an obvious change from dark to light with carbonation time, which is more pronounced for 0.3 M STPP-containing binder. It is worth noting that the fading time of pink color is prolonged with the increase of STPP amount, indicating the extension of carbonation reaction controlled by STPP. After 72 h carbonation, no obvious alteration in color can be observed, which may be attributed to the main completeness of carbonation reaction [6]. Different from STPP-containing mixes, all control samples without STPP present white color due to the non-hydraulic property of wollastonite.

Fig. 4 illustrates the compressive strength development of carbonated wollastonite composites with STPP content increasing from 0 to 0.3 M. It can be found that the addition of STPP improves the compressive strengths of carbonated composites, attributed to the crystallization controlling effect of STPP for $CaCO_3$ polymorph [6,44]. 0.1 M STPP-containing composites exhibit the highest strengths, which are 69.17 MPa and 75.59 MPa at 3 and 28-day curing age, respectively, showing 83.71% and 74.53% growths in comparison with that of the control mix. As the STPP content increases, the compressive strengths of

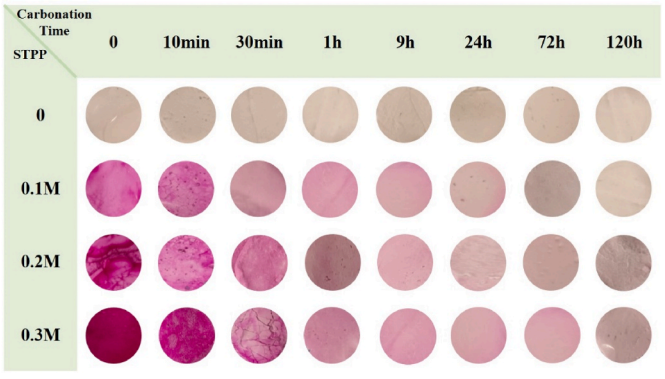

Fig. 3. The color variation indicated by phenolphthalein pH-indicator as a function of carbonation time and STPP concentration. (For interpretation of the references to color in this figure legend, the reader is referred to the Web version of this article.)

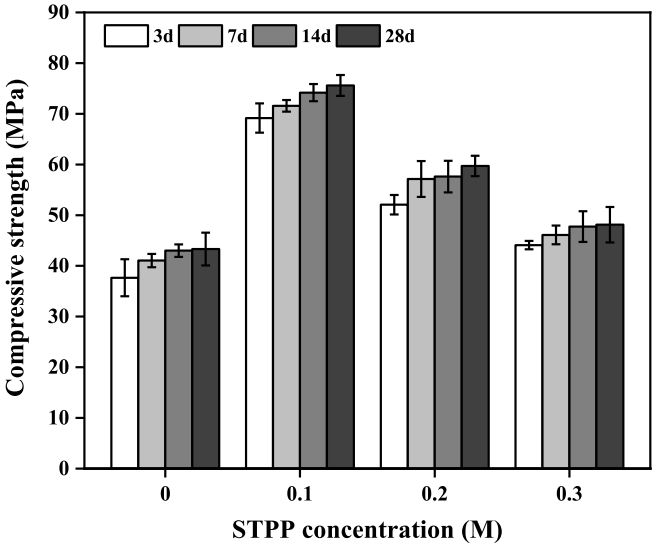

Fig. 4. Compressive strength of carbonated composites after different carbonation ages.

0.2 M and 0.3 M STPP-containing composite decrease. Nevertheless, their strengths still reach 37.84% and 11.10% higher than that of control binder at 28-day carbonation. As such, the concentration range of STPP within 0.3 M is conducive to compressive strength growth. On the other hand, these composites show excellent compressive strength at 3 days while they only show a slight increase with the extension of carbonation duration from 3 to 28 days. This originates from the early-curing rapid carbonation and late-curing hinders CO_2 diffusion into the hardened matrix [48]. Furthermore, the density and workability results (Fig. S1, Supplementary Materials) show that the density and workability first increases and then decreases with the addition of STPP, consistent with the development trend of compressive strength.

3.2. Identification and evolution of $CaCO_3$ phases

Fig. 5 presents FTIR spectra of all samples at different carbonation durations, and the detailed infrared absorption bands of $CaCO_3$ polymorphs are presented in Table 2. For raw wollastonite, the absorption band at or below 700 cm^{-1} corresponds to the out-of-plane skeletal (v_4) and in-plane skeletal (v_2) vibrations of Si-O bond; while the broad peak between 800 cm^{-1} and 1200 cm^{-1} corresponds to the asymmetrical stretching vibration (v_3) of the Si-O bond [49,50]. Due to the fact that the symmetric stretch (v_1) of $CaCO_3$ polymorphs at around 1080 cm^{-1} is overlapped by the v_3 peak of the Si-O bond, this peak is not used for $CaCO_3$ polymorph identification in composites.

From Fig. 5a, it can be observed that the control sample contains ACC at 30min carbonation, which is identified by the broad peak at 1432 cm^{-1}, due to the v_3 vibration of CO_3^{2-} group. At 1h carbonation, phase transition of ACC occurs and crystallizes to calcite, demonstrated by the shift and narrowing of the v_3 peak at 1428 cm^{-1}. In addition to this, the sharp in-plane bending (v_4) at 712 cm^{-1} and the out-of-plane bending (v_2) at 876 cm^{-1} also confirm the presence of calcite polymorph. These peaks related to calcite become stronger with the exposure time to CO_2. A small peak at about 856 cm^{-1} is observed after 72 h, which is the characteristic of aragonite [51]. Besides, the carbonation reaction of wollastonite leads to the silicate polymerization and the formation of silica gel [52], which is reflected by the shift of v_3 vibration of the Si-O-Si bond at 1085 cm^{-1} and 1190 cm^{-1} to a higher wavenumber [53].

Different from the structural rearrangement of the control sample at 1h, the addition of STPP can stabilize more ACC (namely, stable ACC) and retard the phase transition reaction of ACC until 72 h later, observed by the shift of v_3 band from broad peak of ACC to 1428 cm^{-1} of calcite

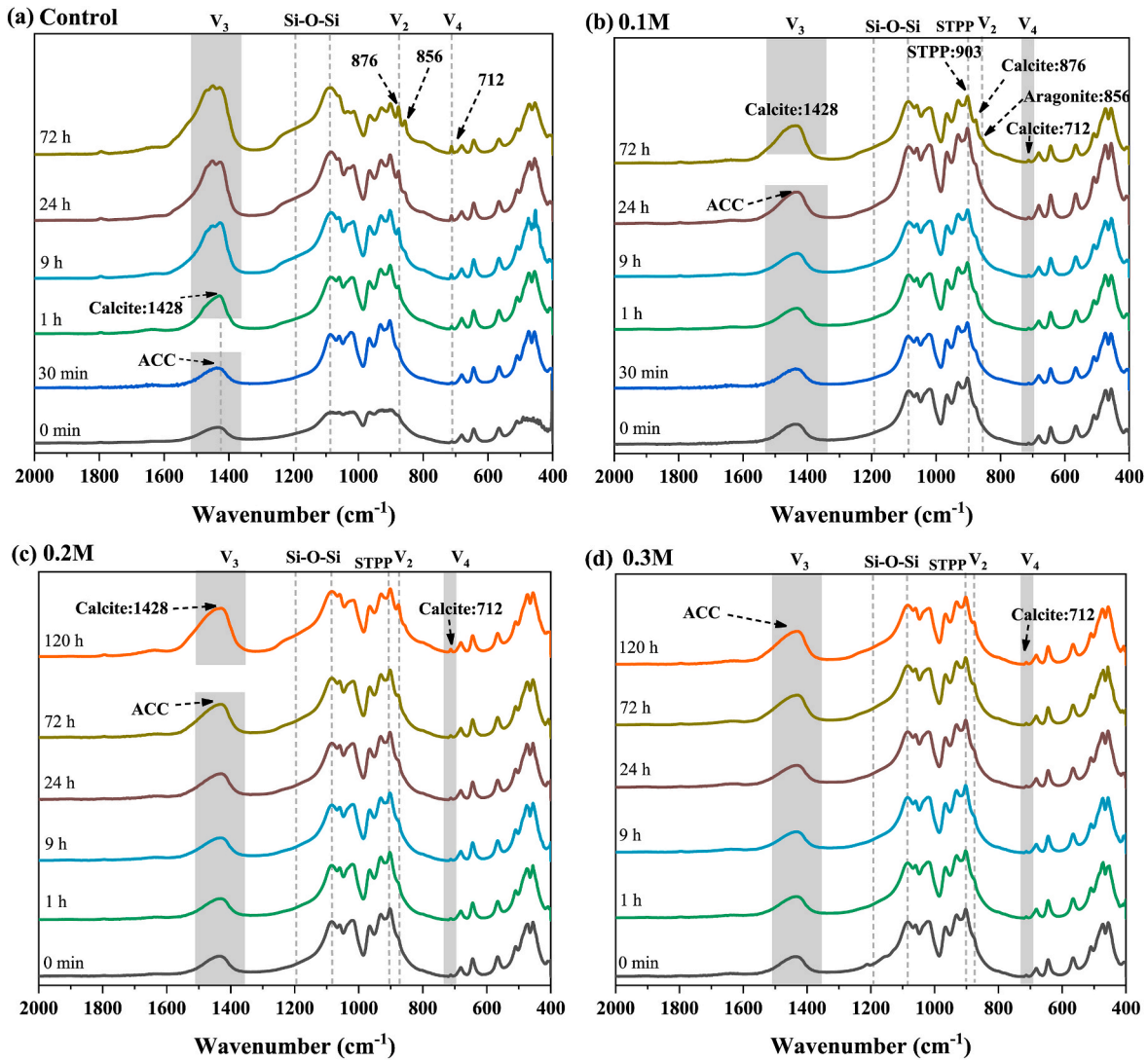

Fig. 5. FTIR spectra of carbonated wollastonite composites in the presence of (a) 0, (b) 0.1 M, (c) 0.2 M, (d) 0.3 M STPP.

Table 2
Wavenumbers (cm^{-1}) of FTIR absorption bands for $CaCO_3$ polymorphs.

$CaCO_3$ polymorphs	Symmetric stretch (v_1)	In-plane bending (v_2)	Stretching vibration (v_3)	Out-plane bending (v_4)
ACC	1067	866	1420 to 1480	Absent or broad peak
Vaterite	1088	878	1495,1433,1412	744
Aragonite	1084	856	1506,1450	713
Calcite	1080	876	1421,1429 (relatively narrow)	712

(as shown in Fig. 5b–d). Before 72 h carbonation, the v_3 band of STPP-containing binder exhibits a broad peak in the range of 1420 cm^{-1} to 1480 cm^{-1}, representing the characteristics of transient ACC and metastable vaterite. The typical absorption bands at 712 cm^{-1} of calcite also provide evidence for the phase transformation behavior of ACC during the whole reaction, including transient ACC before 72 h and stable ACC after 72 h carbonation. Furthermore, a strong shift signal of STPP is observed (from 897 cm^{-1} to 903 cm^{-1}), indicating that STPP regulates the phase transition reaction of ACC and $CaCO_3$ crystals by incorporating or adsorbing on the outer layer of particles [6].

In terms of 0.1 M STPP-containing sample, the absorption bands shift from the broad peak of ACC to 1028 cm^{-1} of calcite, indicating the phase change behavior of ACC at 72h. At 120 h carbonation, a small peak located at 856 cm^{-1} indicates the presence of aragonite. In the meantime, the bands of 1450 cm^{-1} and 1428 cm^{-1} gradually dominate and strengthen, implying the formation of a large amount of $CaCO_3$ and the enhancement of carbonation reaction [5]. For 0.2 M STPP-containing sample, a broad peak shows the presence of stable ACC at 72 h carbonation while the peak of calcite at 1429 cm^{-1} is observed at 120 h carbonation, indicating that stable ACC has experienced phase transition (Fig. 5c). Unlike the above cement, ACC and vaterite are observed in 0.3 M STPP samples at all tested ages (Fig. 5d). As a result, ACC, vaterite, and calcite are the primary components of $CaCO_3$ in the 0.3 M STPP-containing composites. The XRD results (Fig. S2, Supplementary Materials) support the experimental finding of FTIR spectra. A prominent reduction in the peak intensity of calcite with increased STPP can be found. This is ascribed to the fact that STPP adsorbed on the particle surface provides more crystallization sites [54], which favors the formation of ACC. Therefore, the carbonation reaction, including the phase transition of ACC and $CaCO_3$ polymorph evolution, strongly depends on the amount of STPP. As STPP content increases, structural rearrangement of $CaCO_3$ is prolonged and the relative proportion of poorly crystalline phase (ACC, vaterite, and aragonite) increases.

3.3. Relative quantification of carbonated products and its binder efficiency

3.3.1. TG results

TGA technology is used to determine the relative proportions of different $CaCO_3$ polymorph and silica gel with carbonation duration. The weight loss of different binder with carbonation duration are shown in Fig. 6. Based on previous studies [55,56], TGA plots are divided into three main parts: (1) The evaporation of free water and dehydration of silica gel occurred before 200 °C. (2) The temperature range of 200 °C to 350 °C is regarded as the characteristic indicator of chemically bound water. This weight loss is attributed to the dehydration brought by $CaCO_3$ crystallization transformation [44]. (3) Major weight loss due to the decarbonization of $CaCO_3$ occurs in the temperature range of 350 °C to 800 °C. Then, poorly crystalline $CaCO_3$ (ACC, vaterite, and aragonite) decomposes at a lower decomposition temperature of 350 °C to 650 °C [22,57]. The main decrease in weight is centered in the temperature range of 650 °C to 800 °C, which is resulted from the decarbonation of well crystalline $CaCO_3$ polymorph (calcite) [58]. The decomposition temperature of calcite increases with carbonation duration while it decreases with increased STPP content.

3.3.2. Carbonation degree and relative quantification of carbonated products

Further, the mass ratio of poorly crystalline $CaCO_3$, calcite, and silica gel in STPP-modified materials at different carbonation duration are presented in Fig. 7. The amounts of poorly crystalline $CaCO_3$, calcite, and silica gel increase with the carbonation time. The increase rate of all carbonated products is fast in the first 3 days, while the rate significantly slows down with carbonation time from 3 days to 28 days, which is consistent with the development of compressive strength (Fig. 4). Meanwhile, with the increased content of STPP, poorly crystalline $CaCO_3$ increases and calcite decreases, indicating that the existence of STPP can inhibit the phase transition from ACC to calcite. Silica gel decreases as STPP content increases. These results demonstrate that STPP-containing binder has more poorly crystalline $CaCO_3$, less calcite and less silica gel.

The relative proportion of poorly crystalline $CaCO_3$ to the total carbonate is calculated by the ratio of 'weight loss from 350 °C to 650 °C' to 'weight loss from 350 °C to 800 °C', as shown in Fig. 8a. It is clear that the incorporation of STPP greatly increases the quantity of poorly crystalline $CaCO_3$. Moreover, all samples show high poorly crystalline $CaCO_3$ content at the early stage of carbonation that gradually reduces with carbonation duration. This is ascribed to the fact that transient ACC is the first to nucleate, which then transforms into metastable vaterite or aragonite, and finally, forms the most stable calcite [59]. Additionally, an interesting phenomenon is observed in STPP-containing material that the relative proportion of poorly crystalline $CaCO_3$ reaches the lowest level at 3d and then continues to decrease. It manifests that stable ACC (with more STPP) dehydrates into vaterite or calcite [6], which favors the enhancement of carbonation reaction from 3 to 28 days.

Moreover, the weight loss from 350 °C to 800 °C is used to calculate the amount of total $CaCO_3$ formed in the binder, and the degree of carbonation (DOC) is calculated using Eq. (3) and the corresponding results are given in Fig. 8b.

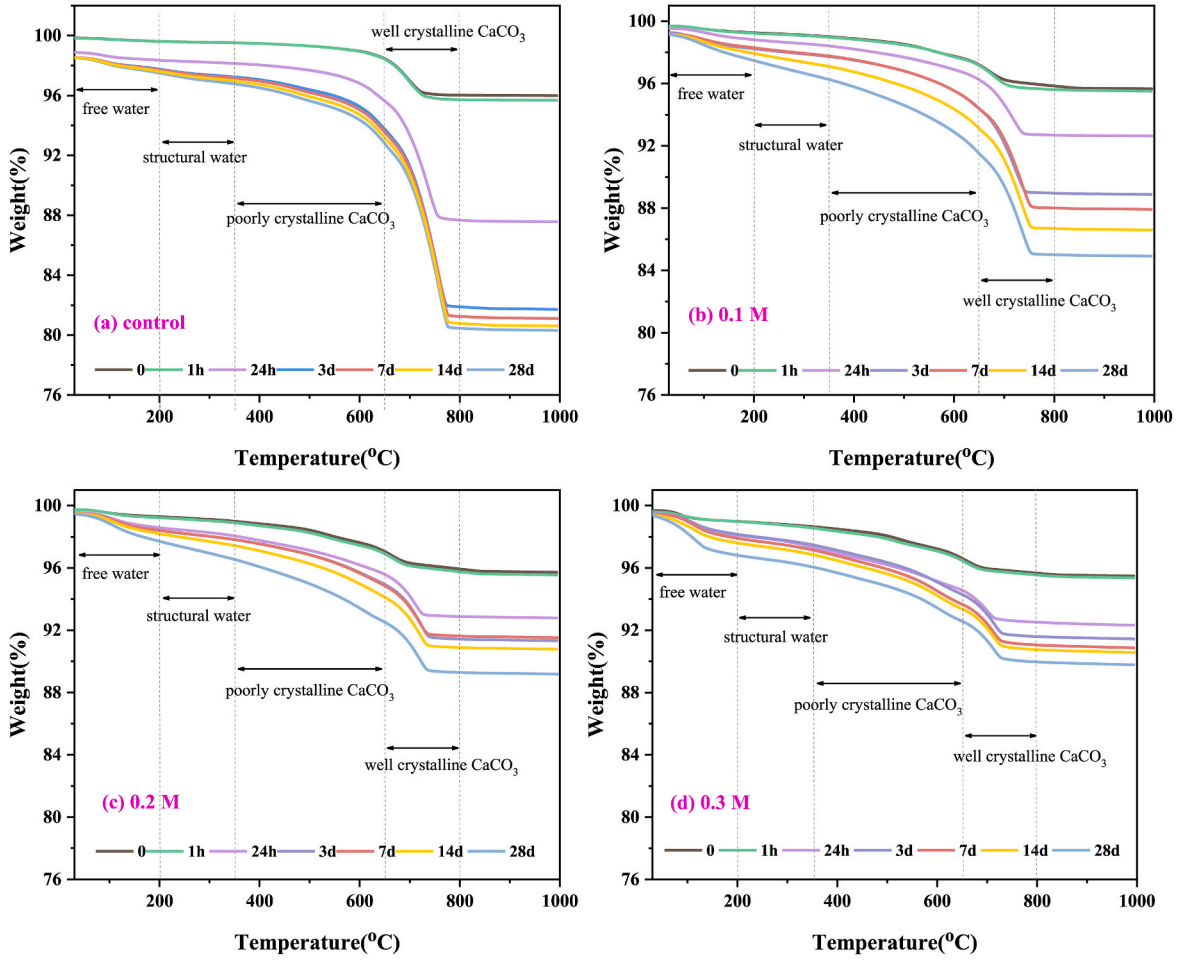

Fig. 6. TG plots of carbonated wollastonite composites after different carbonation duration.

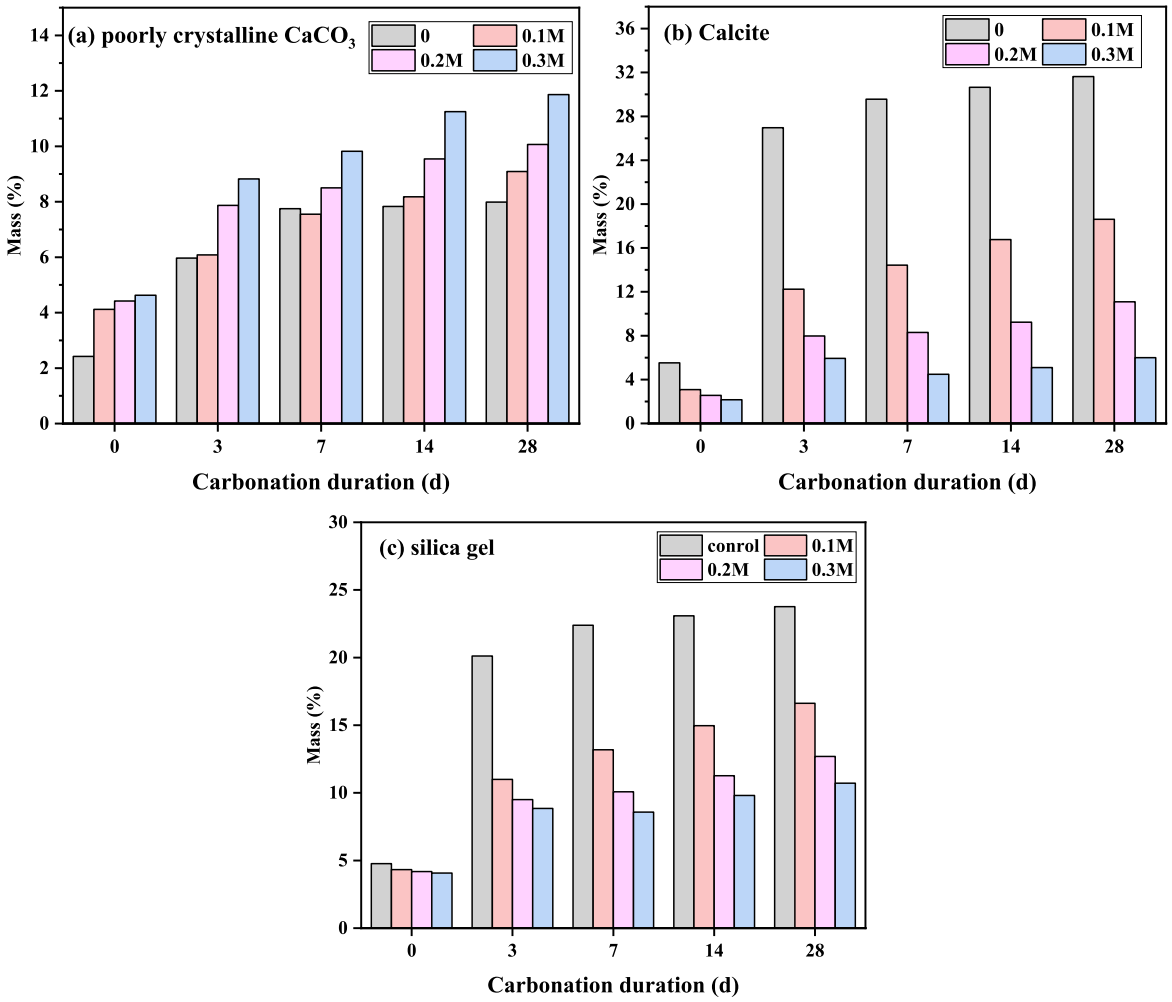

Fig. 7. The mass ratio of carbonated products in different STPP-containing composites with carbonation duration.

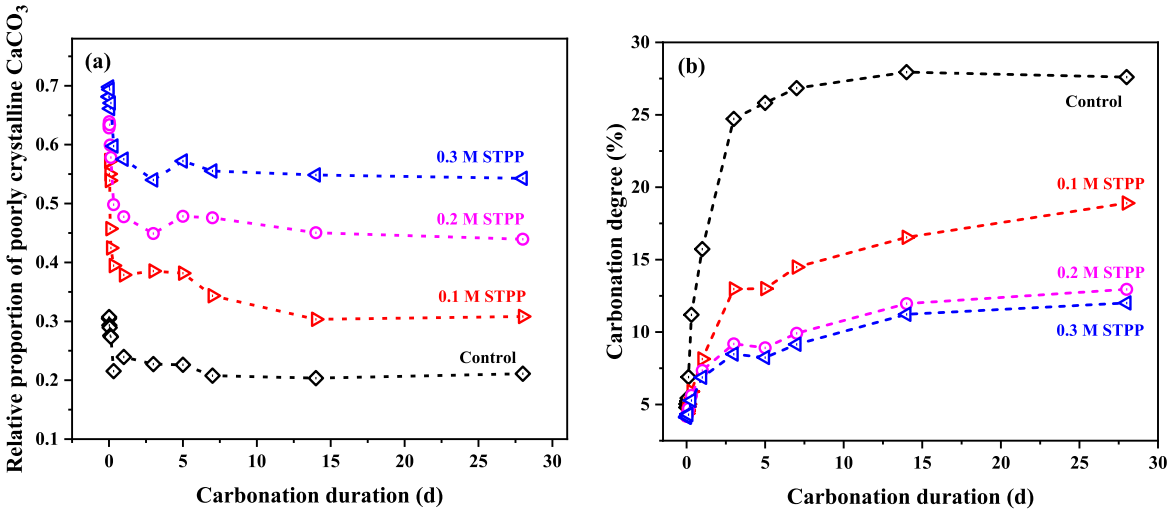

Fig. 8. (a) The proportion of poorly crystalline $CaCO_3$ and (b) the degree of carbonation with carbonation duration, respectively.

$$DOC = \frac{m_{CO2}}{m_{CO2\ max}} \quad (3)$$

Where m_{CO2} is the mass of CO_2 decomposed from cement upon heating (refer to the mass of CO_2 absorbed in the carbonation process). $m_{CO2\ max}$ is the theoretical maximum CO_2 absorption of wollastonite, which is based on XRF results and calculated by Eq. (4). m_0 is the mass of wollastonite before carbonation. The molar mass of wollastonite and CO_2 are 116 and 44 g/mol, respectively.

$$m_{CO2\ max} = m_0 \times \frac{2 \times M_{CO2}}{M_{wollastonite}} = \frac{22}{29} m_0 \quad (4)$$

As can be observed from Fig. 8b, the incorporation of STPP leads to a lower carbonation degree compared to the control sample under the same carbonation duration. Specifically, 0.2 M and 0.3 M STPP-containing binders have the lowest carbonation degree after 28 days carbonation, and the carbonation degree of control sample is twice that of the 0.1 M STPP-containing binder. Combined with Fig. 8a, it is observed that a higher amount of poorly crystalline $CaCO_3$ results in a lower carbonation degree in this system.

3.3.3. Relationship between compressive strength and carbonated products

As discussed in previous sections, compressive strength is closely related to the amounts of carbonated products and carbonation duration. According to the above results, the relationship between compressive strength and carbonated products (poorly crystalline $CaCO_3$, calcite, and silica gel), is used to draw radar diagrams in control and STPP-containing (0.1 M) binder, as shown in Fig. 9. The mass percentages of carbonated products are calculated based on the percentage of each component's mass in the total mass of three components. At 3 days carbonation (Fig. 9a), the silica gel amount is almost the same in binders without and with STPP. After 0.1 M STPP is added, the ratio of poorly crystalline $CaCO_3$ increases, but calcite decreases. These variations correspond to increased compressive strength, indicating the enhancement of compressive strength is related to increased poorly crystalline $CaCO_3$. At 28 days carbonation (Fig. 9b), the relationship between compressive strength and carbonated products is the same at 3 days. However, due to the low stiffness effect of poorly crystalline $CaCO_3$ [29] and decreased carbonation degree (Fig. 8b), excessive poorly crystalline phase reduces compressive strength in 0.2 and 0.3 M STPP-containing binders. Fig. S3 (Supplementary Materials) demonstrates the optimal ratio of poorly crystalline $CaCO_3$, calcite and silica gel is about 9:19:17 in 0.1 M STPP-containing sample.

Furthermore, to study the contribution of carbonated products on compressive development controlled by STPP, the binder efficiency is calculated using Eq. (5). The binder efficiency is defined as normalized compressive strength at 3 and 28 days by binder mass percent, and the result is shown in Fig. 10. Where σ_c and m_{binder} are the compressive strength and the corresponding carbonated products, respectively.

$$X = \sigma_c / m_{\text{binder}} \quad (5)$$

Based on the above analysis, the introduction of STPP results in the formation of more poorly crystalline $CaCO_3$ (ACC, vaterite, and aragonite) by controlling phase transition of ACC. As observed from Fig. 10, the binder efficiency of all carbonated products is much higher than the control sample for STPP-containing sample, meaning the strength not only comes from the formation of calcite and silica gel, but also the transition from ACC to other $CaCO_3$ polymorphs. Therefore, the difference of binder efficiency between STPP-containing and control binders at the same carbonation duration demonstrates cementitious performance resulting from ACC phase transition (Fig. 10a). From Fig. 10b–d, the cementitious performance of all carbonated products increases significantly. Specifically, the cementitious efficiency of poorly crystalline $CaCO_3$ increases first and then decreases with the increased STPP, and the cementitious efficiency of 0.1 M STPP is the highest in the range of 8–9 MPa/% (Fig. 10b). Compared to the control sample, the binder efficiencies of calcite and silica gel in STPP-containing samples are improved by 2–3 times (Fig. 10c and d). Subsequently, with the increase of STPP concentration, the cementitious efficiencies of calcite and silica gel slowly increase and decrease, respectively.

These phenomena persuasively testify that the addition of STPP plays a significant role in $CaCO_3$ polymorph evolution controlled by phase transition of ACC and contributes to the compactness of hardened matrix, although the carbonation degree of STPP-containing binder is lower than the control sample. This effect can be attributed to the following reasons:

(i) STPP is incorporated in $CaCO_3$ or adsorbed on the surface of wollastonite, resulting in a reduction of surface area available for carbonation reaction. This reduction of reaction sites leads to a lower carbonation degree for STPP-containing composites (Fig. 8b). Besides, the pH value of carbonated materials tends to increase with increased STPP (Fig. 4). When the same amount of CO_2 enters the carbonated matrix, these materials with more STPP need to consume more CO_2 to participate in the neutralization reaction, thus, less CO_2 is available for the carbonation

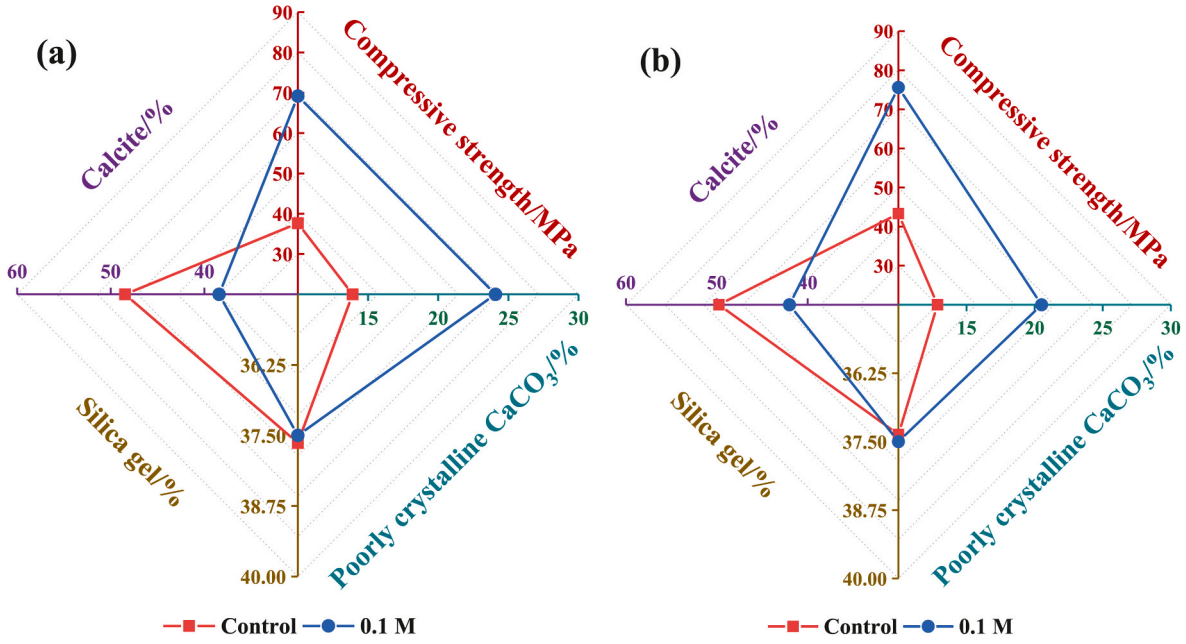

Fig. 9. Relationship between compressive strength and carbonated products (mass percentage) in control and 0.1 M STPP-containing binders at (a) 3 days and (b) 28 days carbonation.

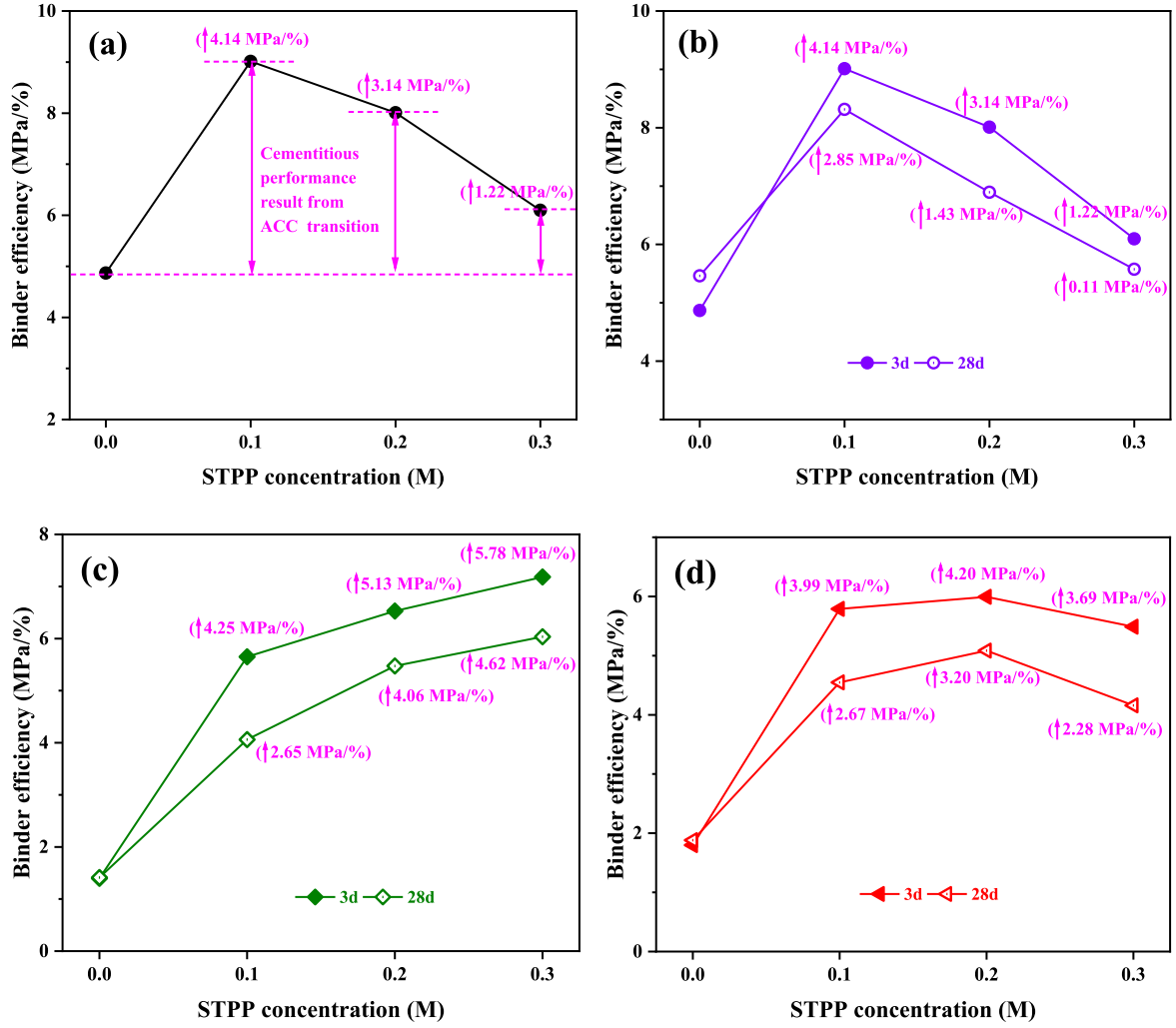

Fig. 10. (a) calculation method of cementitious performance, (b), (c) and (d) binder efficiency of poorly crystalline $CaCO_3$, calcite, and silica gel, respectively.

reaction. In these cases, carbonation degree decreases with STPP concentration.

(ii) The addition of STPP provides more crystallization site, thereby stabilizing more poorly crystalline $CaCO_3$ (Fig. 8a) and then favoring the reduction of poorly crystalline $CaCO_3$ size [60]. Due to less ordered property, poorly crystalline $CaCO_3$ with smaller size merge in several locations, which generates a binding capacity to the matrix (as seen from Fig. 12). Owing to the higher solubility of ACC (ACC is 120 times more soluble than calcite), this phase can transform into a unique cross-linked structure by altering the crystallization pathways [61–63]. Then, the increased poorly crystalline phases surround solid particles and bind them, thereby, the finest cementitious cross-linked structure is formed, which makes a significant contribution to the development of the compact structure. Therefore, the compressive strength of STPP-containing binder is higher than that of the control sample without STPP (Fig. 4).

(iii) The densities of $CaCO_3$ polymorphs are: ACC~1.62–2.59 g/cm^3, vaterite ~ 2.66 g/cm^3, aragonite ~ 2.93 g/cm^3, calcite ~ 2.71 g/cm^3 [64]. On the condition of the same mass, the volume of poorly crystalline phases increases compared with well crystalline phases [5]. Thus, the binding effect of increased poorly crystalline phase (ACC, vaterite) densifies matrix of this binder and further refines pore structure (Fig. 14). As a result, CO_2 diffusion is mitigated in the matrix, leading to a lower carbonation degree (Fig. 8b). Considering carbonation degree to be a significant source of compressive strength of the carbonated matrix, hence, excessive reduction of carbonation degree is responsible for decreased compressive strength as STPP amount increase from 0.1 M to 0.3 M.

3.4. Morphology and pore structure

Fig. 11 exhibits the SEM images of wollastonite without treatment and after immersing in 0.1 M STPP solution for 60 days. From Fig. 11a-b, ground wollastonite particles have different sizes, with the majority of them being irregular with relatively sharp edges. A small number of the particles show rod-like shape with a large aspect ratio, which is mainly owing to the crystal structure of wollastonite and the applied processing technique [65]. Further, fine $CaCO_3$ particles adhere to the surface of wollastonite powder. After the wollastonite is immersed in 0.1 M STPP solution (Fig. 11c-d), rod-like particles disappear and the crystal structure becomes compact, implying the rearrangement of wollastonite.

The SEM images are used to study the effect of STPP on the $CaCO_3$ polymorph formed in carbonated wollastonite composites, as shown in Fig. 12. From Fig. 12a, the control sample shows a well-defined shape (including rhombohedral calcite, and rod-like aragonite), and the crystal size is in the range of 200–600 nm. After adding STPP, $CaCO_3$ crystal shapes disappear or are wrapped, then irregular shapes are tightly interconnected, as shown in Fig. 12b-d. This may be ascribed to increased poorly crystalline $CaCO_3$ (less ordered, observed in Figs. 7 and 8)), resulting in the formation of cementitious behavior [66]. In the case

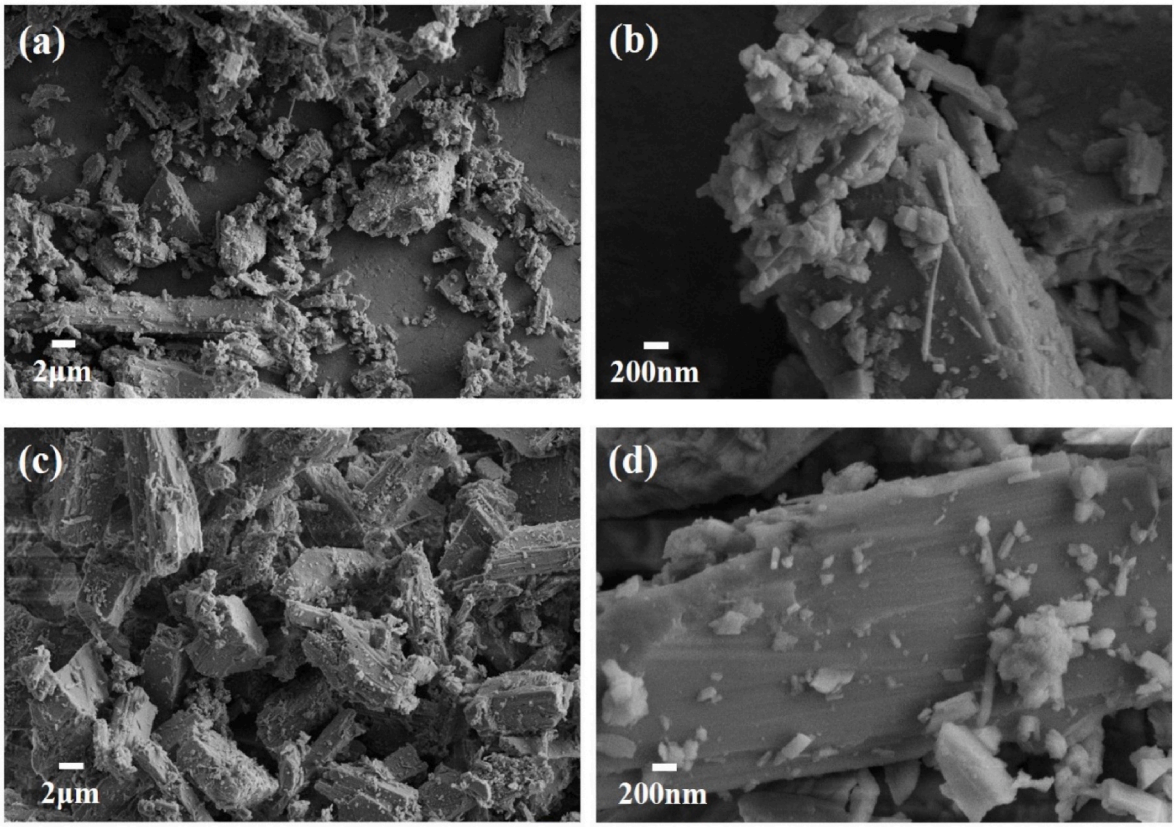

Fig. 11. SEM images of wollastonite (a-b) without any treatment and (c-d) with immersing in 0.1 M STPP solution for 60 days.

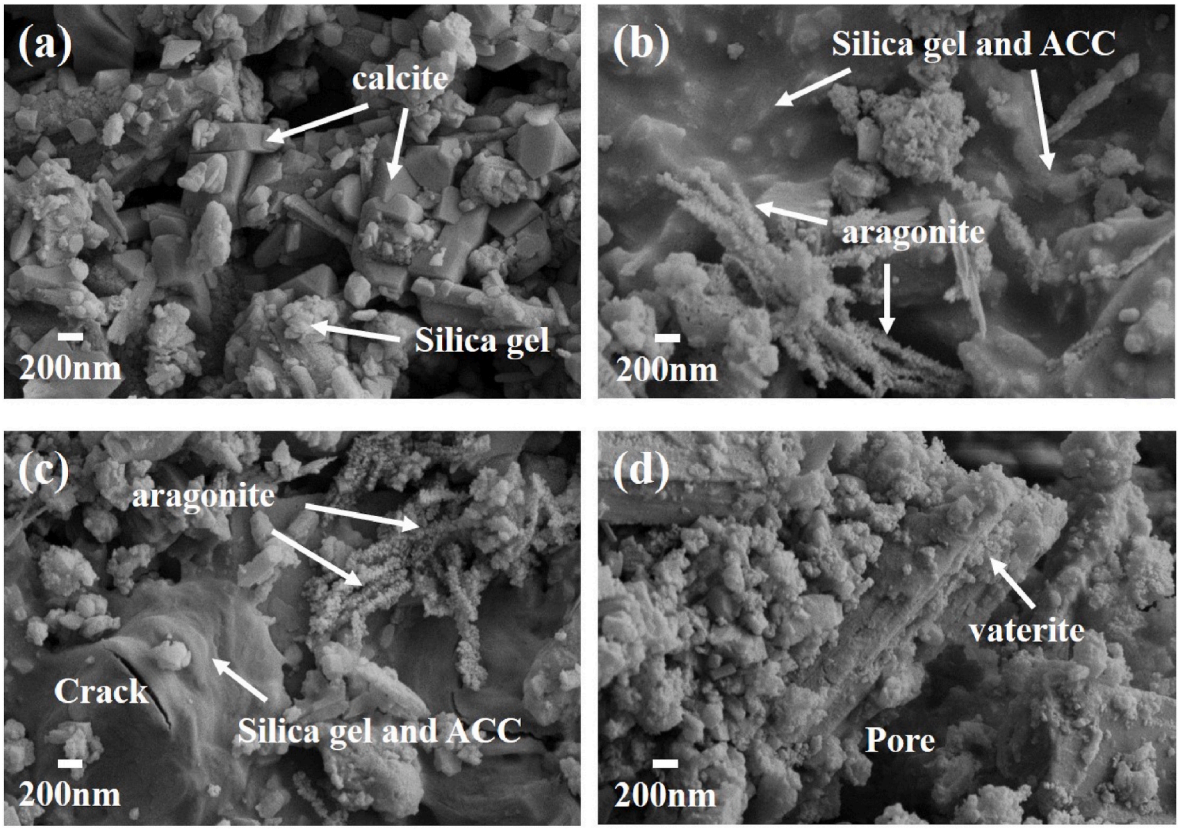

Fig. 12. SEM images of binder (a) control sample, (b) with 0.1 M STPP, (c) with 0.2 M STPP, (d) with 0.3 M STPP.

of 0.1 M STPP-containing binder, more disordered $CaCO_3$ particles merged in several locations, which gives a binding capacity to the matrix [5,6], thus, the cross-linked structure is observed (Fig. 12b). Moreover, the sizes of $CaCO_3$ and silica gel significantly decrease. The formation of aragonite is apparent from the presence of rod-like $CaCO_3$. With the incorporation of STPP (0.2 M and 0.3 M STPP), the spherical $CaCO_3$ particles (ACC and vaterite) increase, and subsequently, a slight swell and large pores are observed (Fig. 12c-d). Noteworthy, the microstructure of binder containing 0.3 M STPP is highly variable, and the parallel arrangement of vaterite plates results in the formation of layer-like structure [5].

Fig. 13 shows the microstructures and EDS results of 0.1 M STPP-containing cementitious material. The distribution of carbonated products forms a matrix with the dispersion of Ca, C, P, and Si. The $CaCO_3$ are readily identified from the C and Ca, which indicates the uniform distribution of $CaCO_3$ in the connected location of solid particles (can also be observed from Fig. 13c and d). The map of P suggests that STPP is distributed throughout the matrix, which is in agreement with the FT-IR results of Fig. 5. From SEM images of Fig. 13a and b, noticeably reduced cracks and almost no large pores can be observed with the addition of 0.1 M STPP, which can provide support for greatly reduced pore size (see MIP results in Fig. 14). The unreacted wollastonite grains are coated with carbonated products and further fill into pores to refine the microstructure, making a visible effect in 0.1 M STPP-containing binder.

It is widely acknowledged that the refinement of pore structure can be one of the explanations for the development of mechanical properties [67]. The results of MIP are presented in Fig. 14 to investigate the effect of STPP amount on the pore structure of carbonated wollastonite composites. Compared to the control sample, the pore size of STPP-containing binder is finer and the total pore volume is lower. Specifically, the addition of STPP decreases the critical pore size (size of the pore with maximum volume) and the median pore sizes (sizes for which 50% of the pores are smaller and 50% are larger) of the carbonated composites. The critical pore diameters of the control, 0.1 M, 0.2 M and 0.3 M samples are 454 nm, 329 nm, 330 nm and 363 nm, respectively. The median pore sizes of the control, 0.1 M, 0.2 M and 0.3 M samples are 361 nm, 235 nm, 296 nm and 321 nm, respectively. Due to the nucleation effect of STPP, more poorly crystalline $CaCO_3$ (e.g. ACC and vaterite) are formed, which makes the occurrence of structural rearrangement, brought by phase transition. This leads to a binding behavior and more compact microstructure of carbonated composites [5,68]. Nevertheless, with the STPP content increasing from 0.1 M to 0.3 M, the carbonated composite exhibits increased pore volume in the range of 0.1–1 μm.

4. Discussion

4.1. Cementitious mechanism of carbonated binder

As observed in Results section, all STPP-containing binders form more poorly crystalline $CaCO_3$, including ACC, vaterite, and aragonite, controlled by the phase transition of ACC and $CaCO_3$ polymorph evolution. Based on the principle of biomineralization, the presence of STPP inhibits the transition from metastable $CaCO_3$ to a stable polymorph (calcite). Specifically, the interaction between STPP and Ca^{2+} prolongs the phase transition of ACC (from 1 h of control sample to 72 h of STPP-

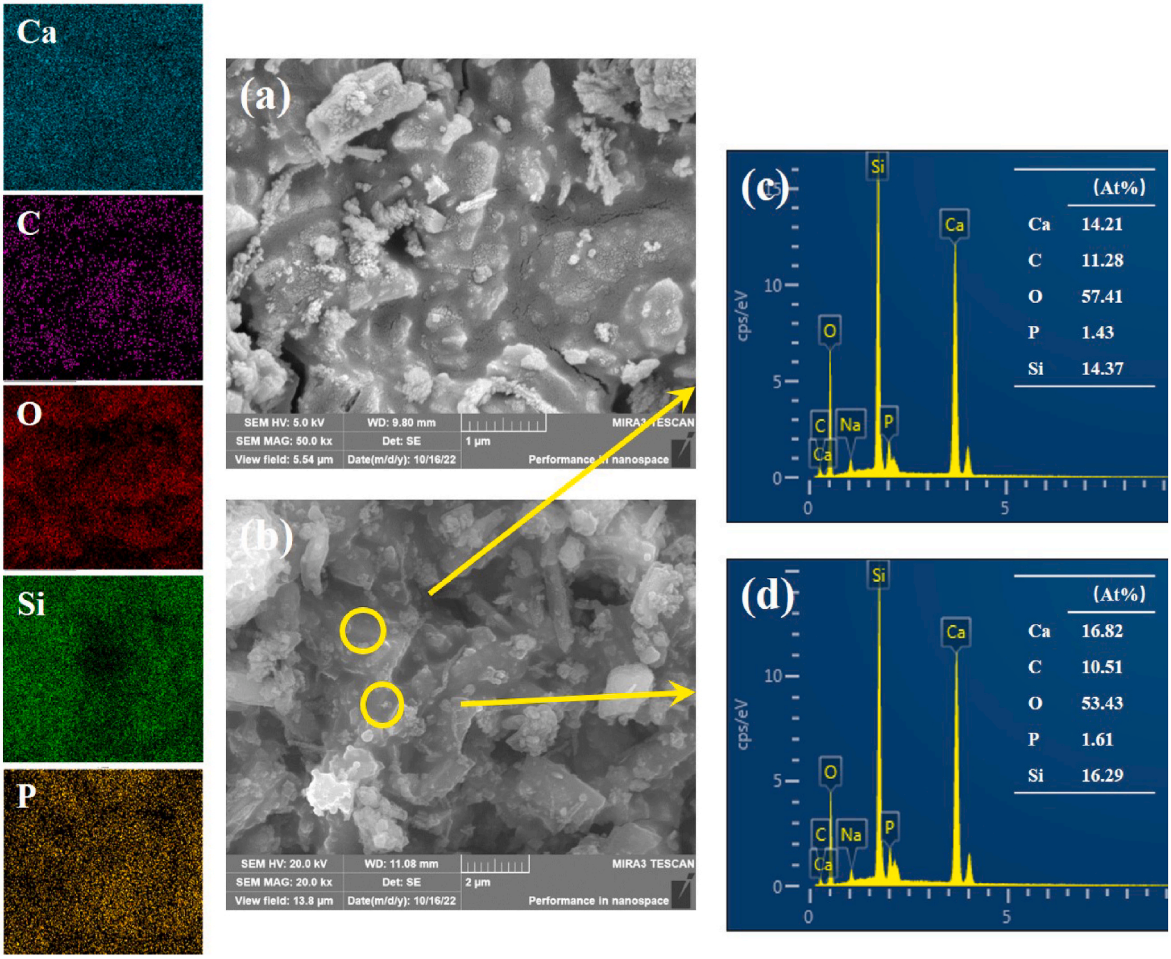

Fig. 13. Microstructures and chemical composition of 0.1 M STPP-containing binder.

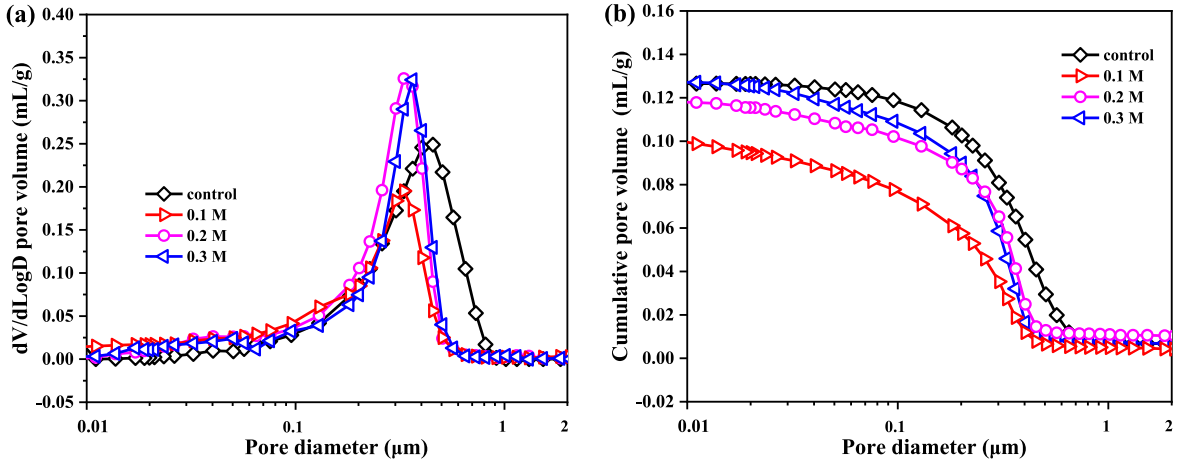

Fig. 14. (a) Pore size distribution and (b)cumulative pore volume.

containing sample, as shown in Fig. 5) and results in the stabilization of more poorly crystalline $CaCO_3$ (Fig. 8a). The carbonation mechanism of this matrix in the presence of STPP is summarized in Fig. 15. In the initial stage of carbonation reaction, some transient ACC (with less STPP) is immediately formed and is assembled to form $CaCO_3$ crystalline by classical dissolution-recrystallization mechanism. At this point, the first carbonation reaction (approximately 3 days in duration) has achieved about 90% of its maximum degree of compressive strength, which is rapid and depends on the specific surface area of ground wollastonite [48]. As the carbonation duration increases to 3 days (Figs. 5 and 8a), stable ACC (with more STPP) initiates the phase transition [6], which is responsible for the slight increase of compressive strength from 3 to 28 days (Fig. 4). On these conditions, the $CaCO_3$ grows into a cross-linking structure that bonds the surrounding solid particles together to create a compact matrix (Fig. 12). The phase transition of ACC results in the increased binder efficiency of all carbonated products and a higher strength of binders with STPP, even though it decreases carbonation degree. This effect shows the most visible effect in 0.1 M STPP-containing binder. Therefore, the carbonation process of carbonated composites is similar to a natural mechanism known as rock

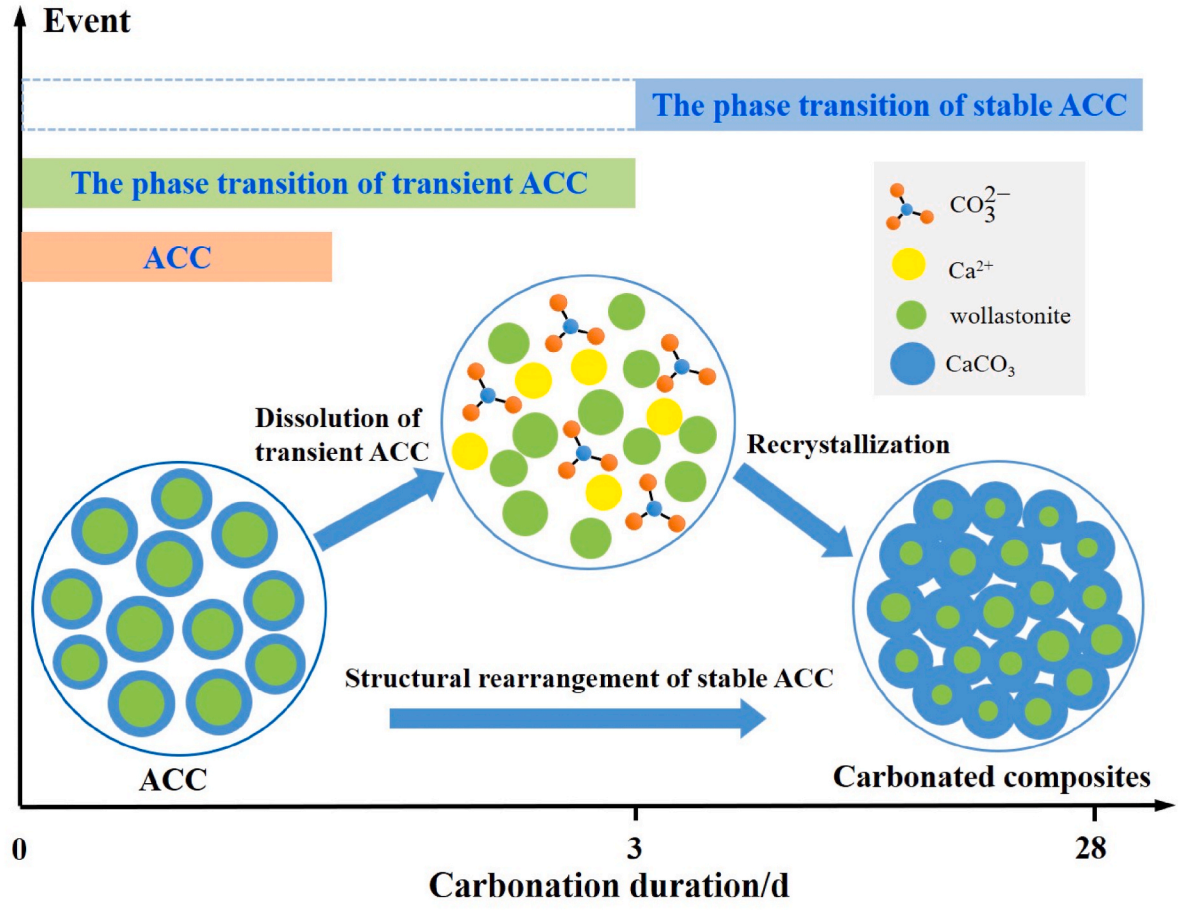

Fig. 15. The cementitious mechanism of carbonated wollastonite composites.

weathering that sequesters atmospheric CO_2 and obtains the limestone-like cementitious material [16,69,70].

4.2. Energy consumption and carbon footprint

The cradle-to-gate method is used to analyze CO_2 emissions and energy consumption during the life cycle of various STPP-containing carbonated wollastonite composites. The system involves the acquisition and transport of raw materials, as well as the manufacture of binder products. Carbonated products are prepared in the laboratory scenario. The detailed calculation method, data source and further assumptions are shown in Supplementary Information. Table 3 compares the energy consumption and carbon footprint of the proposed carbonated binder and conventional Portland cement (PC) during the life cycle analysis. The functional unit is 1 ton of material. From Tables 3, it can be found that carbonated wollastonite composites have a distinct reduction in total energy consumption and total CO_2 emissions per unit weight than those of PC. Also, the increasing dosage of STPP in the binder decreases energy consumption and CO_2 absorption. Focusing on CO_2 absorption, this binder is carbon-negative while total CO_2 emissions are positive, as noted in Table 3. Such phenomenon results from the maximum amount of CO_2 reabsorbed by this system is less than the amount released during carbonation production. Although carbonation curing process consumes CO_2 (up to 379.31 kg CO_2 per ton of wollastonite for 100% conversion to $CaCO_3$), the whole process from grinding carbon-free feedstock material to the carbonation curing, is powered by electricity. Comparing with the high energy consumption and CO_2 emissions of traditional Portland cement, carbonated wollastonite composites are significantly attractive.

Table 3
Comparison of energy consumption and CO_2 emissions of carbonated wollastonite composites and conventional Portland cement.

	Carbonated wollastonite composites				PC
	0	0.1 M	0.2 M	0.3 M	
Total Energy consumption (kJ/ton of cement)	3.6×10^5	8.7×10^5	7.7×10^5	4.6×10^5	3.8×10^6
CO_2 absorption (kg/ton of cement)	−175.9	−89.4	−66.0	−64.1	0
Total CO_2 emissions (kg/ton of cement)	148.13	128.25	123.56	122.03	793

5. Conclusions

In the present study, novel carbonated wollastonite composites are prepared by controlling the phase transition of $CaCO_3$ in the presence of sodium tripolyphosphate (STPP), and the influences of STPP on the performance development and carbonation mechanism of this binder are investigated. The major conclusions can be drawn below:

(1) STPP is effective in controlling the phase transition of $CaCO_3$ by affecting phase transition duration and polymorphs. On the one hand, STPP prolongs the phase transition of ACC until 72 h later (the control sample at 1h), allowing more opportunities for structural rearrangement. Specifically, transient ACC (with less STPP) is assembled to form $CaCO_3$ within 3 days while stable ACC (with more STPP) transforms to vaterite, aragonite, or calcite after 3 days. On the other hand, the introduction of STPP results in the formation of more poorly crystalline $CaCO_3$ (stable ACC, vaterite, and aragonite) in carbonated wollastonite composites. This variation leads to a compact microstructure and a lower carbonation degree, which is attributed to the adsorption of STPP on the surface of wollastonite and the difference of various $CaCO_3$ phases in density and disorder properties.

(2) $CaCO_3$ phase transition is beneficial for the enhancement of mechanical property. The cementitious performance resulting from $CaCO_3$ phase transition is characterized as the difference of binder efficiency between STPP-containing and control binders at the same carbonation duration. STPP concentration within 0.3 M strongly improves cementitious performance of all carbonated products (2.65–4.14 MPa/%), contributing to compressive strength growth (11.10–83.71 %). The 0.1 M STPP-containing binder exhibits the highest binder efficiency and compressive strength of 75.59 MPa, showing a 75% increase compared to the control sample without STPP.

(3) Under the control of $CaCO_3$ phase transition, structural rearrangement of increased poorly crystalline $CaCO_3$ occurs and the microstructure is refined. Due to the nucleation effect of STPP, the size of these phases (less ordered) decreases, which merges in several locations and generates a binding capacity to the matrix. The unreacted wollastonite grains are coated with carbonated products and fill into pores to refine the microstructure. Further, the pore size of STPP-containing binder is finer and the total pore volume is lower, namely, the addition of STPP decreases the critical pore size and the median pore size of the carbonated composites.

CRediT authorship contribution statement

Lulu Cheng: Data curation, Formal analysis, Investigation, Methodology, Writing – original draft. **Yuxuan Chen:** Investigation, Supervision, Writing – review & editing. **Tao Liu:** Investigation. **H.J.H. Brouwers:** Investigation. **Qingliang Yu:** Conceptualization, Funding acquisition, Investigation, Methodology, Project administration, Resources, Supervision, Writing – review & editing.

Declaration of competing interest

The authors declare that they have no known competing financial interests or personal relationships that could have appeared to influence the work reported in this paper.

Data availability

Data will be made available on request.

Acknowledgments

This research was carried out under the funding of the Knowledge Innovation Program of Wuhan-Basic Research (NO. 2023020201010076), National Natural Science Foundation of China (Grant No. 52178246), and Provincial Key Research and Development Plan (2023BAB105).

Appendix A. Supplementary data

Supplementary data to this article can be found online at https://doi.org/10.1016/j.cemconcomp.2024.105477.

References

[1] W. Ashraf, J. Olek, J. Jain, Microscopic features of non-hydraulic calcium silicate cement paste and mortar, Cement Concr. Res. 100 (2017) 361–372, https://doi.org/10.1016/j.cemconres.2017.07.001.
[2] P. Badjatya, A.H. Akca, D.V. Fraga Alvarez, B. Chang, S. Ma, X. Pang, E. Wang, Q. van Hinsberg, D.V. Esposito, S. Kawashima, Carbon-negative cement manufacturing from seawater-derived magnesium feedstocks, Proc. Natl. Acad. Sci. U.S.A. 119 (2022) 1–10, https://doi.org/10.1073/pnas.2114680119.
[3] C. Shi, B. Qu, J.L. Provis, Recent progress in low-carbon binders, Cement Concr. Res. 122 (2019) 227–250, https://doi.org/10.1016/j.cemconres.2019.05.009.
[4] S. Liu, Y. Shen, Y. Wang, P. Shen, D. Xuan, X. Guan, C. Shi, Upcycling sintering red mud waste for novel superfine composite mineral admixture and CO2 sequestration, Cem. Concr. Compos. 129 (2022) 104497, https://doi.org/10.1016/j.cemconcomp.2022.104497.

[5] R.I. Khan, W. Ashraf, J. Olek, Amino acids as performance-controlling additives in carbonation-activated cementitious materials, Cement Concr. Res. 147 (2021) 106501, https://doi.org/10.1016/j.cemconres.2021.106501.

[6] L. Cheng, Y. Chen, B. Yuan, Q. Yu, The underlying role of sodium tripolyphosphate on the cementitious mechanism of calcium carbonate binder, Composites, Part B (2022) 110362, https://doi.org/10.1016/j.compositesb.2022.110362.

[7] C. Combes, B. Miao, R. Bareille, C. Rey, Preparation, physical-chemical characterisation and cytocompatibility of calcium carbonate cements, Biomaterials 27 (2006) 1945–1954, https://doi.org/10.1016/j.biomaterials.2005.09.026.

[8] C. Combes, S. Tadier, H. Galliard, S. Girod-Fullana, C. Charvillat, C. Rey, R. Auzély-Velty, N. El Kissi, Rheological properties of calcium carbonate self-setting injectable paste, Acta Biomater. 6 (2010) 920–927, https://doi.org/10.1016/j.actbio.2009.08.032.

[9] M.C.G. Juenger, F. Winnefeld, J.L. Provis, J.H. Ideker, Advances in alternative cementitious binders, Cement Concr. Res. 41 (2011) 1232–1243, https://doi.org/10.1016/j.cemconres.2010.11.012.

[10] W. Ashraf, J. Olek, Carbonation behavior of hydraulic and non-hydraulic calcium silicates: potential of utilizing low-lime calcium silicates in cement-based materials, J. Mater. Sci. 51 (2016) 6173–6191, https://doi.org/10.1007/s10853-016-9909-4.

[11] J. Chang, T. Jiang, K. Cui, Influence on compressive strength and CO2 capture after accelerated carbonation of combination β-C2S with γ-C2S, Construct. Build. Mater. 312 (2021) 125359, https://doi.org/10.1016/j.conbuildmat.2021.125359.

[12] P. De Silva, L. Bucea, D.R. Moorehead, V. Sirivivatnanon, Carbonate binders: reaction kinetics, strength and microstructure, Cem. Concr. Compos. 28 (2006) 613–620, https://doi.org/10.1016/j.cemconcomp.2006.03.004.

[13] Y.X. Chen, G. Liu, K. Schollbach, H.J.H. Brouwers, Development of cement-free bio-based cold-bonded lightweight aggregates (BCBLWAs) using steel slag and miscanthus powder via CO2 curing, J. Clean. Prod. 322 (2021), https://doi.org/10.1016/j.jclepro.2021.129105.

[14] S. Kerisit, E.J. Bylaska, A.R. Felmy, Water and carbon dioxide adsorption at olivine surfaces, Chem. Geol. 359 (2013) 81–89, https://doi.org/10.1016/j.chemgeo.2013.10.004.

[15] H. Huang, R. Guo, T. Wang, X. Hu, S. Garcia, M. Fang, Z. Luo, M.M. Maroto-Valer, Carbonation curing for wollastonite-Portland cementitious materials: CO2 sequestration potential and feasibility assessment, J. Clean. Prod. 211 (2019) 830–841, https://doi.org/10.1016/j.jclepro.2018.11.215.

[16] W. Ding, H. Yang, J. Ouyang, H. Long, Modified wollastonite sequestrating CO2 and exploratory application of the carbonation products, RSC Adv. 6 (2016) 78090–78099, https://doi.org/10.1039/c6ra13908f.

[17] W. Ashraf, J. Olek, S. Sahu, Phase evolution and strength development during carbonation of low-lime calcium silicate cement (CSC), Construct. Build. Mater. 210 (2019) 473–482, https://doi.org/10.1016/j.conbuildmat.2019.03.038.

[18] W. Ashraf, J. Olek, Elucidating the accelerated carbonation products of calcium silicates using multi-technique approach, J. CO2 Util. 23 (2018) 61–74, https://doi.org/10.1016/j.jcou.2017.11.003.

[19] Z. Zou, W.J.E.M. Habraken, G. Matveeva, A.C.S. Jensen, L. Bertinetti, M.A. Hood, C.-Y. Sun, P.U.P.A. Gilbert, I. Polishchuk, B. Pokroy, J. Mahamid, Y. Politi, S. Weiner, P. Werner, S. Bette, R. Dinnebier, U. Kolb, E. Zolotoyabko, P. Fratzl, A hydrated crystalline calcium carbonate phase: calcium carbonate hemihydrate, Science 363 (2019) 396–400, 80-.

[20] Z. Zou, W.J.E.M. Habraken, G. Matveeva, A.C.S. Jensen, L. Bertinetti, M.A. Hood, C. Sun, P.U.P.A. Gilbert, I. Polishchuk, B. Pokroy, J. Mahamid, Y. Politi, S. Weiner, P. Werner, S. Bette, R. Dinnebier, U. Kolb, E. Zolotoyabko, P. Fratzl, A hydrated crystalline calcium carbonate phase: calcium carbonate hemihydrate, Science 363 (2019) 396–400, https://doi.org/10.1126/SCIENCE.AAV0210, 80-.

[21] X. Xu, J.T. Han, D.H. Kim, K. Cho, Two modes of transformation of amorphous calcium carbonate films in air, J. Phys. Chem. B 110 (2006) 2764–2770, https://doi.org/10.1021/jp055712w.

[22] J. Ihli, W.C. Wong, E.H. Noel, Y.Y. Kim, A.N. Kulak, H.K. Christenson, M.J. Duer, F. C. Meldrum, Dehydration and crystallization of amorphous calcium carbonate in solution and in air, Nat. Commun. 5 (2014) 1–10, https://doi.org/10.1038/ncomms4169.

[23] F.M. Michel, J. MacDonald, J. Feng, B.L. Phillips, L. Ehm, C. Tarabrella, J.B. Parise, R.J. Reeder, Structural characteristics of synthetic amorphous calcium carbonate, Chem. Mater. 20 (2008) 4720–4728, https://doi.org/10.1021/cm800324v.

[24] Y. Politi, T. Arad, E. Klein, S. Weiner, L. Addadi, Sea urchin spine calcite forms via a transient amorphous calcium carbonate phase, Science 306 (2004) 1161–1164, https://doi.org/10.1126/science.1102289, 80-.

[25] M.H. Nielsen, S. Aloni, J.J. De Yoreo, In situ TEM imaging of CaCO3 nucleation reveals coexistence of direct and indirect pathways, Science 345 (2014) 1158–1162, https://doi.org/10.1126/science.1254051, 80-.

[26] Y. Politi, Y. Levi-Kalisman, S. Raz, F. Wilt, L. Addadi, S. Weiner, I. Sagi, Structural characterization of the transient amorphous calcium carbonate precursor phase in sea urchin embryos, Adv. Funct. Mater. 16 (2006) 1289–1298, https://doi.org/10.1002/adfm.200600134.

[27] Y.U.T. Gong, C.E. Killian, I.C. Olson, N.P. Appathurai, A.L. Amasino, M.C. Martin, L.J. Holt, F.H. Wilt, P.U.P.A. Gilbert, Phase transitions in biogenic amorphous calcium carbonate, Proc. Natl. Acad. Sci. U.S.A. 109 (2012) 6088–6093, https://doi.org/10.1073/pnas.1118085109.

[28] Y. Politi, R.A. Metzler, M. Abrecht, B. Gilbert, F.H. Wilt, I. Sagi, L. Addadi, S. Weiner, P. Gilbert, Transformation mechanism of amorphous calcium carbonate into calcite in the sea urchin larval spicule, Proc. Natl. Acad. Sci. U.S.A. 105 (2008) 17362–17366, https://doi.org/10.1073/pnas.0806604105.

[29] N.K. Dhami, A. Mukherjee, M.S. Reddy, Micrographical, minerological and nano-mechanical characterisation of microbial carbonates from urease and carbonic anhydrase producing bacteria, Ecol. Eng. 94 (2016) 443–454, https://doi.org/10.1016/j.ecoleng.2016.06.013.

[30] F. Wu, X. You, M. Wang, T. Liu, B. Lu, G. Hou, R. Jiang, C. Shi, Increasing flexural strength of CO2 cured cement paste by CaCO3 polymorph control, Cem. Concr. Compos. 141 (2023) 105128, https://doi.org/10.1016/j.cemconcomp.2023.105128.

[31] L. Mo, Y. Hao, Y. Liu, F. Wang, M. Deng, Preparation of calcium carbonate binders via CO2 activation of magnesium slag, Cement Concr. Res. 121 (2019) 81–90, https://doi.org/10.1016/j.cemconres.2019.04.005.

[32] M.S. El-Feky, P. Youssef, A.M. El-Tair, S. Ibrahim, M. Serag, Effect of nano silica addition on enhancing the performance of cement composites reinforced with nano cellulose fibers, AIMS Mater. Sci. 6 (2019) 864–883, https://doi.org/10.3934/matersci.2019.6.864.

[33] B. Lu, P. He, J. Liu, Z. Peng, B. Song, X. Hu, Microstructure of Portland cement paste subjected to different CO2 concentrations and further water curing, J. CO2 Util. 53 (2021) 101714, https://doi.org/10.1016/j.jcou.2021.101714.

[34] X. Wang, M.Z. Guo, T.C. Ling, Review on CO2 curing of non-hydraulic calcium silicates cements: mechanism, carbonation and performance, Cem. Concr. Compos. 133 (2022) 104641, https://doi.org/10.1016/j.cemconcomp.2022.104641.

[35] J. Zhang, R. Zhang, H. Geerlings, J. Bi, A novel indirect wollastonite carbonation route for co2 sequestration, Chem. Eng. Technol. 33 (2010) 1177–1183, https://doi.org/10.1002/ceat.201000024.

[36] L.B. Gower, Biomimetic model systems for investigating the amorphous precursor pathway and its role in biomineralization, Chem. Rev. 108 (2008) 4551–4627, https://doi.org/10.1021/cr800443h.

[37] G. Magnabosco, A.M.M. Condorelli, R. Rosenberg, I. Polishchuk, B. Pokroy, D. Gebauer, H. Cölfen, G. Falini, Non-stoichiometric hydrated magnesium-doped calcium carbonate precipitation in ethanol, Chem. Commun. 55 (2019) 12944–12947, https://doi.org/10.1039/c9cc07087g.

[38] E. Seknazi, S. Kozachkevich, I. Polishchuk, N. Bianco Stein, J. Villanova, J. P. Suuronen, C. Dejoie, P. Zaslansky, A. Katsman, B. Pokroy, From spinodal decomposition to alternating layered structure within single crystals of biogenic magnesium calcite, Nat. Commun. 10 (2019) 1–9, https://doi.org/10.1038/s41467-019-12168-8.

[39] Z. Zou, J. Xie, E. Macías-Sánchez, Z. Fu, Nonclassical crystallization of amorphous calcium carbonate in the presence of phosphate ions, Cryst. Growth Des. 21 (2021) 414–423, https://doi.org/10.1021/acs.cgd.0c01245.

[40] A. Al-Sawalmih, C. Li, S. Siegel, P. Fratzl, O. Paris, On the stability of amorphous minerals in lobster cuticle, Adv. Mater. 21 (2009) 4011–4015, https://doi.org/10.1002/adma.200900295.

[41] W.J.E.M. Habraken, A. Masic, L. Bertinetti, A. Al-Sawalmih, L. Glazer, S. Bentov, P. Fratzl, A. Sagi, B. Aichmayer, A. Berman, Layered growth of crayfish gastrolith: about the stability of amorphous calcium carbonate and role of additives, J. Struct. Biol. 189 (2015) 28–36, https://doi.org/10.1016/j.jsb.2014.11.003.

[42] X. Wang, W. Jia, C. Yang, R. He, F. Jiao, W. Qin, Y. Cui, Z. Zhang, W. Li, H. Song, Innovative application of sodium tripolyphosphate for the flotation separation of scheelite from calcite, Miner. Eng. 170 (2021) 106981, https://doi.org/10.1016/j.mineng.2021.106981.

[43] A.L. Goodwin, F.M. Michel, B.L. Phillips, D.A. Keen, M.T. Dove, R.J. Reeder, Nanoporous structure and medium-range order in synthetic amorphous calcium carbonate, Chem. Mater. 22 (2010) 3197–3205, https://doi.org/10.1021/cm100294d.

[44] S. Kababya, A. Gal, K. Kahil, S. Weiner, L. Addadi, A. Schmidt, Phosphate-water interplay tunes amorphous calcium carbonate metastability: spontaneous phase separation and crystallization vs stabilization viewed by solid state NMR, J. Am. Chem. Soc. 137 (2015) 990–998, https://doi.org/10.1021/ja511869g.

[45] Z. Zou, X. Yang, M. Albéric, T. Heil, Q. Wang, B. Pokroy, Y. Politi, L. Bertinetti, Additives control the stability of amorphous calcium carbonate via two different mechanisms: surface adsorption versus bulk incorporation, Adv. Funct. Mater. 30 (2020) 1–10, https://doi.org/10.1002/adfm.202000003.

[46] S.H. Sonawane, S.P. Gumfekar, S. Meshram, M.P. Deosarkar, C.M. Mahajan, P. Khanna, Combined effect of surfactant and ultrasound on nano calcium carbonate synthesized by crystallization process, Int. J. Chem. React. Eng. 7 (2009), https://doi.org/10.2202/1542-6580.2016.

[47] X. Liu, P. Feng, Y. Cai, X. Yu, C. Yu, Q. Ran, Carbonation behavior of calcium silicate hydrate (C-S-H): its potential for CO2 capture, Chem. Eng. J. 431 (2022) 134243, https://doi.org/10.1016/j.cej.2021.134243.

[48] W. Ashraf, J. Olek, Carbonation activated binders from pure calcium silicates: reaction kinetics and performance controlling factors, Cem. Concr. Compos. 93 (2018) 85–98, https://doi.org/10.1016/j.cemconcomp.2018.07.004.

[49] I.F. Sáez Del Bosque, S. Martínez-Ramírez, M.T. Blanco-Varela, FTIR study of the effect of temperature and nanosilica on the nano structure of C-S-H gel formed by hydrating tricalcium silicate, Construct. Build. Mater. 52 (2014) 314–323, https://doi.org/10.1016/j.conbuildmat.2013.10.056.

[50] M. Yousuf, A. Mollah, D.L. Cocke, J.R. Parga, An infrared spectroscopic examination of cement-based solidification/stabilization systems - Portland types V and IP with zinc, J. Environ. Sci. Heal. Part A Environ. Sci. Eng. Toxicol. 27 (1992) 1503–1519, https://doi.org/10.1080/10934529209375809.

[51] D. Chakrabarty, S. Mahapatra, Aragonite crystals with unconventional morphologies, J. Mater. Chem. 9 (1999) 2953–2957, https://doi.org/10.1039/a905407c.

[52] W. Ashraf, J. Olek, Elucidating the accelerated carbonation products of calcium silicates using multi-technique approach, J. CO2 Util. 23 (2018) 61–74, https://doi.org/10.1016/j.jcou.2017.11.003.

[53] F. Spectroscopy, Structure of calcium silicate hydrate (C-S-H), Near-, Mid-, and Far-Infrared Spectroscopy 48 (1999) 742–748.

[54] G.W. Xiaodeng Yang, Qiang Shen, Research progress of water-soluble macromolecules regulating calcium carbonate crystallization, Wuli Huaxue Xuebao 26 (2010) 2087–2095.
[55] M.A. Islam, A. Pal, B.B. Saha, Experimental study on thermophysical and porous properties of silica gels, Int. J. Refrig. 110 (2020) 277–285, https://doi.org/10.1016/j.ijrefrig.2019.10.027.
[56] J.D. Pellett, S. Dwaraknath, E. Nauka, G. Dalziel, Accelerated Predictive Stability (APS) Applications: Packaging Strategies for Controlling Dissolution Performance, Elsevier Inc., 2018, https://doi.org/10.1016/B978-0-12-802786-8.00018-8.
[57] B.C. Chakoumakos, B.M. Pra, R.P. Koenigs, R.M. Br, Empirically testing vaterite structural models using neutron diffraction and thermal analysis, Nat. Publ. Gr. (2016) 1–8, https://doi.org/10.1038/srep36799.
[58] W. Zhuang, S. Li, Z. Wang, Z. Zhang, Q. Yu, Impact of micromechanics on dynamic compressive behavior of ultra-high performance concrete containing limestone powder, Composites, Part B 243 (2022) 110160, https://doi.org/10.1016/j.compositesb.2022.110160.
[59] R. Ševčík, M. Pérez-Estébanez, A. Viani, P. Šašek, P. Mácová, Characterization of vaterite synthesized at various temperatures and stirring velocities without use of additives, Powder Technol. 284 (2015) 265–271, https://doi.org/10.1016/j.powtec.2015.06.064.
[60] Y.G. Bushuev, A.R. Finney, P.M. Rodger, Stability and structure of hydrated amorphous calcium carbonate, Cryst. Growth Des. 15 (2015) 5269–5279, https://doi.org/10.1021/acs.cgd.5b00771.
[61] B. Myszka, K. Hurle, K. Zheng, S.E. Wolf, A.R. Boccaccini, Mechanical improvement of calcium carbonate cements by: in situ HEMA polymerization during hardening, J. Mater. Chem. B 7 (2019) 3403–3411, https://doi.org/10.1039/c9tb00237e.
[62] L. Wang, Z. Ren, H. Wang, X. Liang, S. Liu, J. Ren, Y. He, M. Zhang, Microstructure-property relationships in cement mortar with surface treatment of microbial induced carbonate precipitation, Composites, Part B 239 (2022) 109986, https://doi.org/10.1016/j.compositesb.2022.109986.
[63] S. Askarinejad, F. Shalchy, N. Rahbar, Role of interphase layers in mechanical properties of nacreous structures, Composites, Part B 225 (2021) 109255, https://doi.org/10.1016/j.compositesb.2021.109255.
[64] M. Saharay, A.O. Yazaydin, R.J. Kirkpatrick, Dehydration-induced amorphous phases of calcium carbonate, J. Phys. Chem. B 117 (2013) 3328–3336, https://doi.org/10.1021/jp308353t.
[65] H. Xue, G. Wang, M. Hu, B. Chen, Modification of wollastonite by acid treatment and alkali-induced redeposition for use as papermaking filler, Powder Technol. 276 (2015) 193–199, https://doi.org/10.1016/j.powtec.2015.02.030.
[66] Z. Zou, L. Bertinetti, Y. Politi, P. Fratzl, W.J.E.M. Habraken, Control of polymorph selection in amorphous calcium carbonate crystallization by poly(aspartic acid): two different mechanisms, Small 13 (2017) 1–11, https://doi.org/10.1002/smll.201603100.
[67] H. Zhu, G. Liang, H. Li, Q. Wu, C. Zhang, Z. Yin, S. Hua, Insights to the sulfate resistance and microstructures of alkali-activated metakaolin/slag pastes, Appl. Clay Sci. 202 (2021) 105968, https://doi.org/10.1016/j.clay.2020.105968.
[68] W. Yuhua, S. Daxiang, W. Liguang, Z. Yulin, Effects of sodium tripolyphosphate and sodium carbonate on the selective flocculation of diasporic-bauxite in the presence of calcium and magnesium ions, Miner. Eng. 24 (2011) 1031–1037, https://doi.org/10.1016/j.mineng.2011.04.027.
[69] A. Santos, J.A. Toledo-Fernández, R. Mendoza-Serna, L. Gago-Duport, N. De La Rosa-Fox, M. Piñero, L. Esquivias, Chemically active silica aerogel - wollastonite composites for CO 2 fixation by carbonation reactions, Ind. Eng. Chem. Res. 46 (2007) 103–107, https://doi.org/10.1021/ie0609214.
[70] C.W. Hargis, I.A. Chen, M. Devenney, M.J. Fernandez, R.J. Gilliam, R.P. Thatcher, Storage (CCUS) Technique, 2021, pp. 1–12.